Equilibration processes in surfaces of the binary alloy Fe-Al

2002 J. Phys.: Condens. Matter 14 4145

(http://iopscience.iop.org/0953-8984/14/16/307)

INSTITUTE OF PHYSICS PUBLISHING JOURNAL OF PHYSICS: CONDENSED MATTER

J. Phys.: Condens. Matter **14** (2002) 4145–4164 PII: S0953-8984(02)34624-1

Equilibration processes in surfaces of the binary alloy Fe–Al

L Hammer, W Meier, V Blum and K Heinz

Lehrstuhl für Festkörperphysik, Universität Erlangen-Nürnberg, Staudtstr. 7, D-91058 Erlangen, Germany

E-mail: l.hammer@fkp.physik.uni-erlangen.de

Received 24 January 2002
Published 11 April 2002
Online at stacks.iop.org/JPhysCM/14/4145

Abstract

The scenario of geometrical relaxation or reconstruction known for the surfaces of elemental solids is enriched by surface segregation in the case of compound surfaces. Both phenomena are consequences of the mere creation of the surface in which atoms in a certain slab assume a new positional and stoichiometric equilibrium state. With emphasis on segregation we describe the equilibration processes involved using data evaluated from Auger electron spectroscopy and quantitative electron diffraction available for the binary alloy $Fe_{1-x}Al_x$ for various values of x and different surface orientations. A model is proposed according to which thermally activated processes restore equilibrium between the top layer and a subsurface atomic slab below much faster than between this slab and the bulk of the sample. Whilst the top layer is always Al enriched, the chemical order of the slab is dictated by the phase diagram, i.e. there is local equilibrium according to the actual stoichiometry. So, a transient structure for a certain Al bulk concentration corresponds to the equilibrium structure of a sample with lower bulk Al content. Surface orientation-dependent features can be easily interpreted via the different arrangements of nearest and next-nearest neighbours. By Al segregation, also precipitates can develop with the surface acting as a nucleation centre, again consistent with the phase diagram and local equilibrium. The features found may be extended to other alloys with one of its constituents segregating to the surface.

1. Surface segregation in alloys

The surfaces of alloys dominate their properties in many respects—e.g., their environmental resistivity when used as a material or their efficiency when employed as a catalyst. Certainly, their geometry and chemical composition must play a crucial role in this connection and not surprisingly therefore, these features have been the subject of numerous investigations of both random and ordered alloys (for recent reviews see e.g. [1, 2]). The surface scenario is much

more complex than for surfaces of elemental metals where, at most, some more or less drastic geometrical restructuring can take place induced by the breaking of bonds at the surface. In the surface of a compound, there can be (and usually is) additional chemical restructuring whereby, at least in the case of random alloys, the average stoichiometry within surface-parallel layers or within a whole slab of them need not to be conserved due to segregation processes. Layer-dependent compositional profiles and some short- and long-range order different from those in the bulk can develop, features on which many investigations have focused. For ordered alloys, mainly the issue of surface termination and possible geometrical reconstruction has been addressed, but there are also reports on segregation effects in those systems (e.g. [3–5]).

However, most reports in the literature consider just the structure and stoichiometry established after some surface preparation procedure, i.e., the dependence on the parameters of this procedure (e.g., the annealing temperature) remains largely unconsidered and it is not clear whether the state investigated relates to thermal equilibrium or not. Also, the surface's transient structures and stoichiometries during its move to thermal equilibrium, i.e. the equilibration process itself, usually are not monitored. It is therefore the purpose of this paper to address both these points. We here concentrate on the Fe–Al alloy for which investigations of the structure and stoichiometry for different annealing temperatures, bulk concentrations and surface orientations are available, as carried out earlier by our group. Whilst we present no new experimental results for a particular surface, we aim to use the wealth of results already published to develop a coherent picture of the equilibration processes in Fe–Al. This might hold also for other alloy surfaces.

2. To what extent can equilibrium be achieved in alloy surfaces?

Generally, the stoichiometry as well as the chemical and geometrical order in the surface of an alloy must be expected to be temperature dependent. Therefore, their investigation should be carried out with the surface in thermal equilibrium, as otherwise the features retrieved would correspond to transition states strongly dependent on the preparation conditions. Yet, this requirement demands rather elevated temperatures (typically far above room temperature), since below that all types of diffusion process usually necessary for thermal equilibration are suppressed. However, most of the experimental methods providing structural information must be performed at or even below room temperature. There can be both technical and physical obstacles as, e.g., in scanning tunnelling microscopy (STM) with thermal drift impeding or even preventing atomic resolution or in low-energy electron diffraction (LEED), where thermal diffuse scattering reduces beam intensities exponentially with temperature. So, there are only a few investigations performed for thermal equilibrium states (see, e.g., [6–8]). In the majority of studies the samples are quenched to the low temperatures necessary for the measurement and so the stoichiometry and geometry investigated correspond to an equilibrium state of a certain higher temperature at which, during the quench, the relevant diffusion processes practically freeze in. The latter might even be stepwise when processes with different activation barriers and/or diffusion lengths are involved. Then, the resulting state represents no equilibrium state at all. On the other hand, local atomic rearrangements might not be kinetically limited and then geometrical relaxations, thermal vibrations etc are typical for the temperature of measurement.

Yet, even if the sample temperature at measurement could be freely chosen, the issue of equilibrium remains delicate. Given that it corresponds to a net enrichment of one component at the surface, some mass transport from a region below the surface is necessary which might develop at comparably moderate temperatures as only short-range diffusion is involved (the scenario is given schematically in figure 1). However, this mass transport has to be balanced by some equivalent transport from the crystal's bulk with long-range diffusion involved,

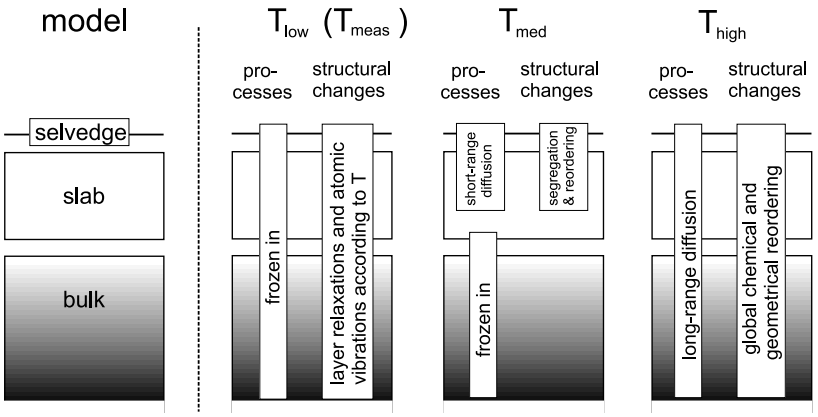

Figure 1. The model of an alloy surface (left). On the right, processes and resulting structural changes developing in the temperature ranges indicated are schematically displayed.

so requiring significantly higher annealing temperatures or much longer annealing periods. So, even in these cases it is difficult to decide whether certain preparation conditions really lead to equilibrium. The situation gets even worse with surface contamination. In particular cases, residual gas-induced structural modifications could be detected after only a few minutes, even at a pressure as low as 10^{-10} mbar [9]. So, long preparation times in the range of days or even months for low-temperature equilibration, routine in bulk metal physics, cannot be allowed for surfaces. Even with much shorter annealing times, there is a risk of adsorbate-induced modifications of the segregation profile, in particular for reactive alloy surfaces, where residual gas components like CO, CO_2 or H_2 can stick even at elevated temperatures. In such cases long- or medium-term annealing must be avoided and so the temperature region available for full equilibration is restricted even further.

Additional difficulties arise from the procedure of cleaning a surface. Only when constituents of low reactivity or alloys with high melting point are involved can surface cleaning be achieved by a simple flash. Already, reactive adsorption/desorption cycles, e.g. annealing in oxygen, lead to adsorbate-induced segregation effects when adsorbates reside intermediately on the surface, though they are removed by a final flash. Even more serious modifications result from ion bombardment frequently used as the first step of *in situ* cleaning and often the only way of getting rid of contaminations in the case of highly reactive samples, e.g. aluminide surfaces (as in the present paper). Additional to elemental intermixing, a selective depletion of one constituent (and enrichment of the other) results within some near-surface regions due to element-dependent sputter yield. This so-called 'altered layer', typically some nanometres thick, must be equilibrated by subsequent annealing involving again high temperatures as long-range diffusion is required. Repeated sputtering can even lead to an altered layer of enormous thickness which can only be removed by mechanical erosion [10]. A similar surface depletion is caused when, after the formation of a surface compound by chemical reaction with the residual gas (e.g. Al_2O_3), the compound is thermally evaporated. At the high temperatures required, usually one of the alloy's components (e.g. Al) preferentially evaporates [11, 12], eventually leading to a rather thick depletion layer (>1 μm) with an (average) depletion of one component by as much as several vol% (e.g. [13][1]).

[1] Prolonged heating of a nominally equiatomic NiAl(100) sample to about 1400 K causes an Al depletion within the near-surface region of the sample equivalent to an average composition $Ni_{0.55}Al_{0.45}$ within the information depth (≈ 1 μm) accessed by energy-dispersive x-ray analysis (EDX).

As described, thermal equilibration between surface and bulk of an alloy is by no means simple, but requires a careful and case-oriented preparation. Moreover, there is no obvious criterion indicating that equilibrium has been reached after a certain preparation step. The only way out is to investigate certain properties of the surface as a function of progressive annealing and to define equilibrium conditions as the asymptotic limit of the data retrieved. Sections 4–6 will give examples for that procedure, preceded by a description of the experimental material on which the present paper is based.

3. Samples considered and experimental access

As already mentioned, we concentrate on various surfaces of Fe–Al alloys. They turn out to be well suited for an exemplary investigation of long-range chemical equilibration. Al is the component expected to segregate preferentially to the surface due to its lower free surface energy [14]. Additionally, argon-ion sputtering—which is the only way to clean the surface, as all other methods fail due to its large reactivity [11]—is pronouncedly preferential, in favour of Al (by about a factor of 3), leading to a drastic reduction of the near-surface Al concentration [11]. So, equilibration must involve a substantial net Al transport from the bulk to the surface. Finally, the phase diagram of Al–Fe [15] shows on the Fe-rich side a sequence of three different phases as a function of Al concentration, namely A2 (=bcc), $D0_3$ and B2 (=CsCl), without significant coexistence regions in between (figure 2(*a*)). A fourth phase, the so-called 'γ-loop' of fcc Fe, can be ignored for the present study, since it appears only at very low Al concentrations and high temperatures. The other three phases differ only in the ratio with which the constituents are distributed within the sublattices of the different structures (figure 2(*b*)). Also, the lattice parameter changes only marginally with stoichiometry [16]. Therefore, the study of equilibration is not complicated by precipitation of completely different phases, and nor do concentration gradients lead to significant dislocations. Thus, mass transport will be dominated by bulk diffusion, while diffusion processes along or across grain boundaries can be assumed to play a minor role.

Samples with different Al bulk concentrations and different surface orientations were available, though not in all combinations. For the (100) surface, random alloys near both the low- and high-concentration edges of the A2 regime (3 and 15 at.% Al, respectively) and ordered in the $D0_3$ regime (30 at.% Al) and the B2 region (47 at.% Al) could be investigated. The (100) surface orientation is favourable because of its low tendency to form superstructures with large unit cells, as known for other low-index surfaces of $Fe_{1-x}Al_x$ [17,18]. As visualized in figure 2(*c*), bulk-terminated (100) surfaces of both the A2 and B2 phases would exhibit a 1×1 periodicity, while for the $D0_3$ phase a c(2×2) superstructure (relative to the bcc host lattice) would result. For the B2-ordered alloy (47 or 50 at.% Al), samples with surface orientations (110), (111), (210) and (310) were also available.

In order to discriminate between elemental rearrangement within the crystal's selvedge driven by surface segregation and full chemical equilibration in the whole surface, experimental methods with information depths not limited to the outermost layer are required. For the present paper, data from both Auger electron spectroscopy (AES) and (in many cases quantitative) LEED were available [3, 11, 18–21]. For a rough overview on the average near-surface composition it is sufficient to monitor the ratio $r_{AES}^{\mathrm{Al/Fe}}$ of peak-to-peak intensities for the low-energy Auger transitions, i.e. Fe(MVV, 48 eV) and Al(LVV, 68 eV). These low-energy lines provide high surface sensitivity due to the small mean free path length of about 4.2 Å [11], a value consistent with both empirical approaches [23,24] and the optical potential [25] fitted in the LEED analyses. With an accuracy in the percentage range, it is a very sensitive measure

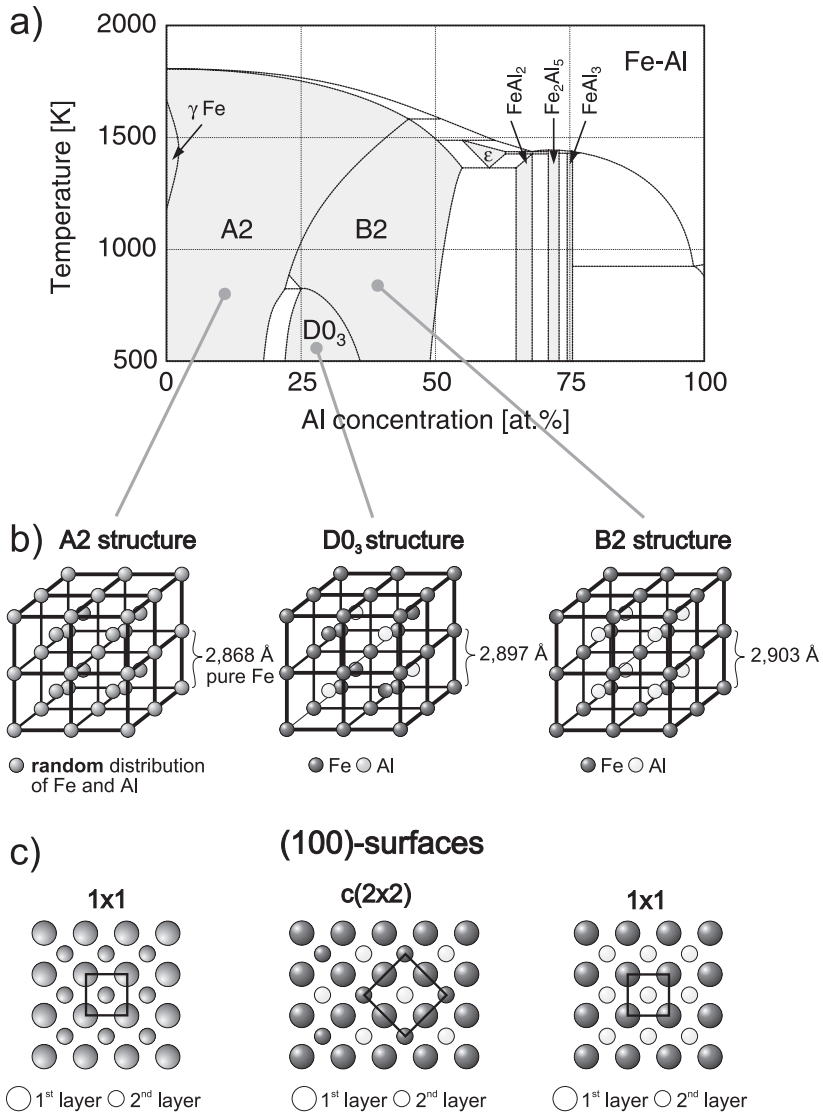

Figure 2. (*a*) The phase diagram of Fe–Al (after [15]), (*b*) lattice types of the Fe-rich regime and (*c*) a view from on top of the corresponding (100) surfaces. Large circles indicate atoms of the first layer, small circles those of the second one.

for the gradual stoichiometric equilibration, as will be used below. Yet, because of the electron attenuation, the elemental concentrations $c_{AES}^{\mathrm{Al,Fe}}$ for the two elements forming the ratio $r_{AES}^{\mathrm{Al/Fe}} \sim c_{AES}^{\mathrm{Al}}/c_{AES}^{\mathrm{Fe}}$ are surface averages exponentially weighted with depth. Certainly, they reflect the vertical elemental distribution, however, not unequivocally—as rather different profiles can lead to the same values for $c_{AES}^{\mathrm{Al,Fe}}$. Of course, $c_{AES}^{\mathrm{Al,Fe}}$ cannot be directly calculated from $r_{AES}^{\mathrm{Al/Fe}}$ but needs the knowledge of the appropriate matrix factor F [26]. Fortunately, this can be determined from the compositional profile known from the quantitative LEED analysis of a certain sample which, besides the surface geometry, retrieves also the layer-dependent stoichiometry. Such an analysis is available for FeAl(100) in the literature [27] and a value

$F = 1.85 \pm 0.15$ can be calculated from it [11]. An increased value was retrieved [18] through the analysis of the same structure by our own group allowing for deviations from the ideal stoichiometry [19], but these deviations were very recently found to be simulated by correlations between chemical and vibrational parameters [20], so the above value of F turns out to be correct. The discussion in section 6 uses calculations of c_{AES}^{Al} based on this value, simultaneously correcting in this respect earlier work [18].

Full dynamical LEED intensity analyses are available for all (100) surfaces [3, 19–21]. In all cases they provide the layer-resolved compositional profile in addition to the geometrical parameters, though the structure determination becomes (compared to that for elemental surfaces) rather laborious with this increased number of parameters [28], and the use of automatic structural search procedures [29] is required. The achievable chemical accuracy depends on the scattering properties of the alloy's components; for the system Fe–Al the error margins for the stoichiometry within a layer are in the region of 5–10% of a monolayer [20, 22].

All surfaces were initially sputtered and then stepwise annealed for short time intervals (typically 2 min) with increasing annealing temperature from step to step (extension of annealing time leads to only minor changes of the surface composition [11]). For the AES and LEED measurements the samples were quenched to room or liquid nitrogen temperature. Annealing was not beyond about 1200 K, where significant amounts of Al begin to evaporate from the surface [11].

4. Local versus global equilibrium

In the following, the annealing paths of the four $Fe_{1-x}Al_x(100)$ surfaces are presented. The development of $r_{AES}^{\mathrm{Al/Fe}}$ with annealing temperature is displayed in figure 3. All samples show a major depletion of Al in the as sputtered state with the depletion gradually lifted in the temperature range 500–900 K. At high temperatures, the Auger ratio saturates at a certain level, which increases with the Al bulk concentration. The development of such plateaus can be taken as evidence that chemical equilibrium of the surface with the bulk has been approached. The saturation is not strictly complete for $x = 0.15$ and 0.30 and the Auger ratio increases again at high temperatures for $x = 0.47$. We ignore this for the moment and come back to it later.

The actual equilibration processes for the different samples are reflected by the transition regimes, where $r_{AES}^{\mathrm{Al/Fe}}$ changes significantly. The onset and end of these ranges can only be defined roughly. As $r_{AES}^{\mathrm{Al/Fe}}$ contains the attenuation-weighted average concentrations c_{AES} and not the real near-surface average c_{av}, it increases as soon as Al starts to segregate towards the selvedge, even if c_{av} might still remain unchanged. In other words, the transition range starts with the onset of near-surface atomic mobility, i.e. not necessarily with that of long-range mass transport (see figure 1). In contrast, it ends in a plateau at the point where the segregation profile accessible to measurement stabilizes as a function of c_{av}. In this sense, the near-surface compositional profiles associated with the high-temperature plateaus in figure 3 are indeed characteristic for full chemical equilibrium with the bulk independent of whether c_{av} has already reached the bulk concentration x or not. The transition ranges as a whole are found to shift towards lower temperatures with increasing x (with the exception of $x = 0.47$ for which at least the plateau is reached at a somewhat higher temperature again). As bulk diffusion shows the same trend [30–32], it seems reasonable to assume that it controls the long-range Al transport necessary for proper equilibration. The different shapes of the curves, however, can be related to both near-surface atomic diffusion processes and the relative amount of net surface segregation as outlined in the next paragraph.

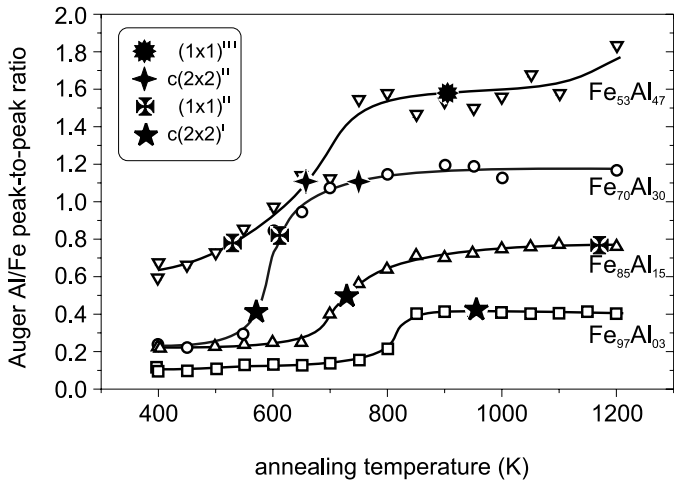

Figure 3. Development of the Auger Al/Fe peak-to-peak ratio, $r_{AES}^{\mathrm{Al/Fe}}$ after initial sputtering as a function of annealing temperature for various $Fe_{1-x}Al_x(100)$ samples. Also indicated are the temperatures of best appearance for the observed ordered intermediate and equilibrium structures.

Let us now add the information on surface order taken from LEED. Right after ion bombardment all samples exhibit 1×1 LEED patterns with rather diffuse and broad diffraction spots indicating severe sputter-induced disorder. With increasing annealing temperature the spots quickly sharpen, indicative for fast local ordering. The well-equilibrated surfaces finally exhibit either 1×1 or c(2×2) LEED patterns. Though this (except for $x = 0.03$) corresponds to the bulk order of the samples (see figure 2(c)), it cannot be taken as a definite indication of a bulk termination of the surfaces. Indeed, the contrary is the case (see section 5).

In the transition ranges, there are various ordered transient states appearing as a function of annealing temperature. Again, all of them are characterized either by 1×1 or c(2×2) periodicities, a finding in agreement with earlier work on related surfaces [8, 33]. This structural information is also added in figure 3 using extra symbols for the different structures at the temperatures of their best appearance. Surprisingly, the LEED patterns for the various structures develop at almost the same Auger ratios $r_{AES}^{\mathrm{Al/Fe}}$ independent of whether they correspond to an intermediate or an equilibrium state. The only exception is the initial 1×1 structure which, however, is produced by sputter-induced chemical intermixing, which corresponds to a rather undefined state frozen in at low temperatures. So, one might ask whether and to what extent the different phases, which develop for the various samples, have common structural elements. This question is easily answered by the comparison of the corresponding LEED intensity spectra, a selection of which are given in figure 4 for integer-order and (where available) fractional-order spots. It is obvious, that—in view of the strong dependence of the spectra on the stoichiometry—the different surface phases denoted by $c(2 \times 2)^{\mathrm{I}}$ or $(1 \times 1)^{\mathrm{II}}$ or $c(2 \times 2)^{\mathrm{II}}$ are indeed identical, irrespective of the sample and annealing temperature at which they appear.

The measurements described suggest the following scenario of the equilibration process (see also figure 1): initial sputtering subdivides the sample into an Al-depleted near-surface region and the remaining crystal (the bulk). Only the surface region is probed by surface-sensitive methods such as AES or LEED because of electron attenuation. Within this altered layer of thickness in the nanometre range, local ordering forces act already at low annealing

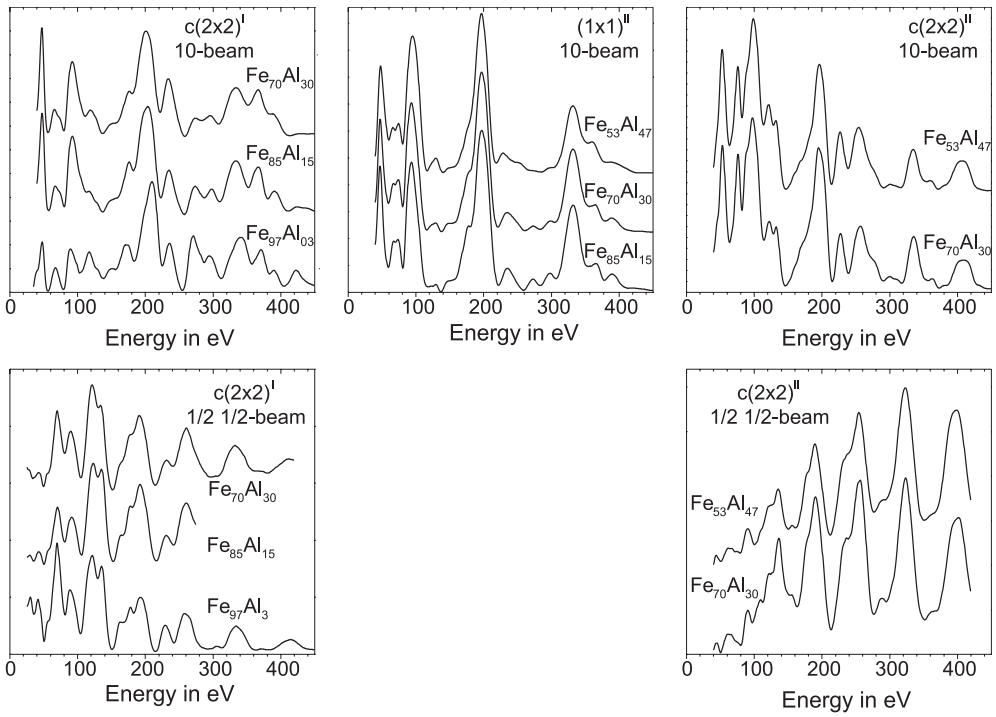

Figure 4. Compilation of LEED intensity spectra for different transient and equilibrium phases developing at the (100) surfaces of various $Fe_{1-x}Al_x$ samples.

temperatures because only short-range diffusion is necessary in the thin slab. As order is determined by only a few short-range interaction parameters (also in the bulk), ordered structures develop within the surface slab consistent with the phase diagram for the actual stoichiometry. These ordering forces also dominate any segregation towards the very surface of the altered layer (which, in turn, could lead to further changes of the average concentration therein). In other words, because little diffusion is necessary to rearrange atoms within the altered layer, the latter develops independently of the distant bulk and easily reaches a state of *local equilibrium*. This is indistinguishable from a true, i.e. *global equilibrium* state of a bulk crystal with a composition equivalent to the actual value within the altered layer. In contrast, long-range chemical equilibration is relatively slow, since it requires a net mass transport over large distances. This is the throttle, which determines the average stoichiometry of the altered layer reached after each annealing step. As a consequence, the equilibration path of the altered layer can be regarded as a continuous motion through a certain region of the phase diagram of the binary alloy system, until it eventually approaches bulk stoichiometry. Since the very surface, i.e. the top layer, is always in equilibrium with the underlying slab, this offers an interesting application: it allows one to deduce the equilibrium surface properties of samples within a whole compositional range from the mere investigation of the equilibration process of one single sample. Vice versa, in cases where true equilibrium structures are known for a variety of bulk compositions, the course of the equilibration can be safely predicted. The rest of the present paper is devoted to these types of application.

Although the above-described scenario was derived for $Fe_{1-x}Al_x$ surfaces only, the underlying mechanisms are supposed to be rather general, i.e. they may well apply to

other alloy surfaces, too. For example, metastable superstructures occurring during stepwise annealing have also been found for sputtered $Pt_3Sn(111)$ [34], NiAl(100) [10,35], TiAl(010) [5] and B2-ordered AlPdMn(110) [36]. Their origin has been mostly attributed to the top layer only, but in the light of the above it is more likely to be due to the local equilibration within a whole, compositionally modified near-surface region. Apparently, this model holds even if the entire underlying lattice needs to be destroyed to reach the state equivalent to the actual near-surface composition: sputter-depleted quasicrystalline (QC) surfaces are commonly reported to form thin films of B2-ordered material with well-defined surface orientations. The original QC lattice is assumed only after subsequent annealing at higher temperatures restoring the overall surface composition [37, 38].

5. From equilibrium structures to the equilibration process—segregation at $Fe_{1-x}Al_x(100)$ surfaces

In the last section, LEED intensity spectra were presented as fingerprints for classifying the various superstructures appearing at certain stages of the equilibration process for samples with different bulk stoichiometries. It was found that transient structures for a certain bulk Al concentration are the same as equilibrium structures observed for samples with lower Al concentration. Therefore, the full dynamical LEED analyses of the equilibrium phases, which yield both the geometric structure and the layer-resolved segregation profiles, provide also access to the same quantities of the transient structures and so to the path of the samples towards equilibrium. This is the focus of the present section. We first recall the results of the LEED structure analyses with emphasis on the layer-dependent stoichiometries (the complete results can be found in the literature [3, 20]) and then address the issue of the equilibration process.

5.1. Layer-dependent concentrations in $Fe_{1-x}Al_x(100)$

Figure 5 compiles schematic models for the best-fit structures which resulted from the LEED analyses. There is only one sample ($x = 0.47$) with a bulk-terminated surface, corresponding to a fully ordered B2 structure with an Al top layer and chemically alternating layers below, as is typical for a B2(100) surface (the limited accuracy of the analysis would hardly allow one to find the small deviation from 1:1 stoichiometry and so this was not taken into account in the LEED analysis [20]). We note that in an earlier study of our group performed for the very same surface [19], some improvement of the theory–experiment fit had been found for an enrichment of Al within the second layer. Yet, this finding was later shown to be a mere artefact of the structural search, which arose from the neglect of an enhanced vibrational amplitude of second-layer atoms [20].

All other samples are found to be strongly enriched in Al at the actual surface, where the *relative* amount of segregation decreases with increasing bulk concentration x. For the Al-poor sample, $Fe_{0.97}Al_{0.03}(100)$, half of the top layer already consists of Al, forming a mixed overlayer of c(2×2) order. The second layer is found to be pure Fe (though the bulk stoichiometry is still well within the limits of error). For the equilibrated $Fe_{0.85}Al_{0.15}(100)$ sample, surface Al concentrations of 75 and 76% were deduced from ion scattering (ISS) and chemically resolved STM studies, respectively [3]. So this could be safely taken as input to the LEED analysis in order to reduce the number of fit parameters. The strong segregation of Al towards the actual surface also leads to a clear Al depletion within the second layer, which is found to be almost pure Fe (5% Al). Finally, the $Fe_{0.70}Al_{0.30}(100)$ surface is determined to be almost completely Al terminated. Therefore, the c(2×2) superstructure observed in the LEED pattern is caused by subsurface order only and has no corresponding feature at the actual surface. Practically the

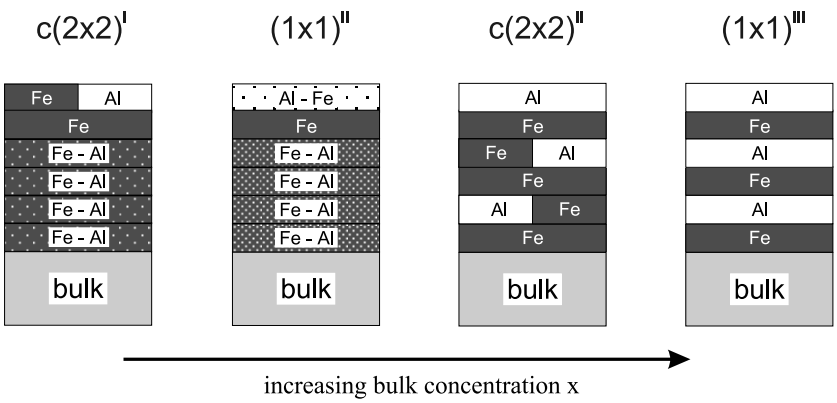

Figure 5. Schematic models for the sequence of phases, which occur as equilibrium states of $Fe_{1-x}Al_x(100)$ surfaces as a function of x. The sequence represents also the intermediate states transited by an initially Al-depleted FeAl(100) surface during its equilibration activated by annealing.

same structure was found earlier for an incompletely annealed $Fe_{0.53}Al_{0.47}(100)$ surface [19], consistent with the equivalence of LEED $I(E)$ spectra as described in the previous section. An unusual feature of this surface is the presence of substitutional defects (10 and 15%) in the outermost two layers retrieved by LEED investigation with correct consideration of atomic vibrations. Though there is no obvious physical reason for any disorder near the surface and the result is only just outside the statistical limits of errors [3], one has to face the fact that x-ray studies of the bulk ordering within the $D0_3$ regime of Fe–Al [39] also found some unexpected chemical disorder among different sublattices actually for $x \approx 0.30$.

5.2. Retrieval of dominating interaction parameters

A global view on the Al segregation at the various bcc-type $Fe_{1-x}Al_x(100)$ surfaces reveals that it clearly proceeds in a two-step mechanism (see figure 6(*a*)). Initially, even for a very dilute distribution of Al in the bulk, half a monolayer of Al segregates to the outermost layer, forming an ordered $c(2 \times 2)$ arrangement. In contrast, the further enrichment of this layer with Al is much slower, with a rate depending approximately linearly on the bulk concentration x (indicating a vanishing segregation enthalpy), until practically full coverage is reached in the $D0_3$ regime. Obviously, such a behaviour cannot be described in the framework of a simple Langmuir–McLean model applying to the segregation of non-interacting particles [40], as both the substantial negative heat of formation [15] and the ordering behaviour of Fe–Al (see figure 2(*a*)) indicate non-negligible, heterogeneous interaction parameters. The occurrence of B2 and $D0_3$ order in the bulk requires attractive interactions of at least nearest (NN) and next-nearest (NNN) neighbours, J_{NN} and J_{NNN}, respectively. Accordingly, an investigation by Sanchez *et al* [41] for bulk $Fe_{0.80}Al_{0.20}$ found that these two interaction parameters are indeed the only relevant ones ($J_{NN} = -23.7$ meV, $J_{NNN} = -7.1$ meV) and so the further discussion can be restricted to them. Though the parameters may be modified at the surface by geometrical and electronic relaxations, their qualitative features should be the same. This appears the more reasonable, as for all samples the structure at the selvedge corresponds to lattice planes of bulk phases with higher Al concentration ($D0_3$ and B2).

A first consequence of the strong attractive heterogeneous NN interaction is that any segregation of Al towards the first layer inevitably leads to an Al depletion in the second layer,

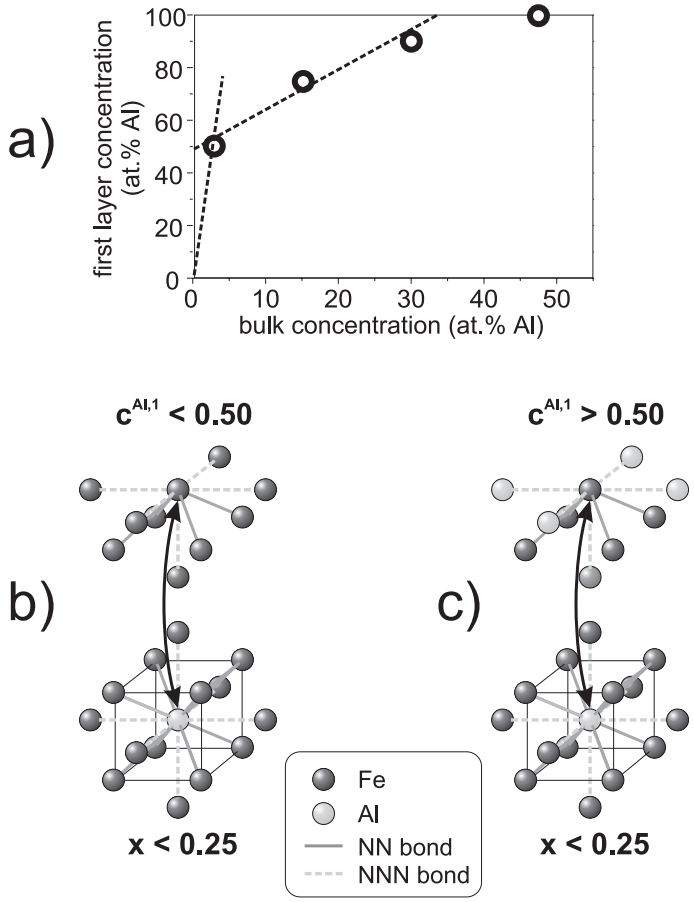

Figure 6. (*a*) The top-layer concentration in $Fe_{1-x}Al_x(100)$ resulting from quantitative LEED investigation. (*b*) Vizualization of the exchange of places between a bulk Al atom and an Fe surface atom for a top-layer coverage $c_{AES}^{Al,1} < 0.5$. (*c*) As (*b*), but for $c_{AES}^{Al,1} > 0.5$.

which is in close accordance with our experimental findings. The energetics of the top-layer Al segregation can be described in such a scenario by simply counting site and bond energies for an exchange of an Fe surface atom with an Al bulk atom. From the strong preference to form heterogeneous bonds it can be expected that up to an Al concentration of $x = 0.25$ a $D0_3$-like short-range (or even long-range) order will exist in the bulk. In other words, every Al atom should be completely surrounded by Fe neighbours in the first and second coordination shells, even in the so-called A2 'random'-alloy regime. So, for both segregation regimes the energetic contribution of the bulk is supposed to be the same and differences in the segregation enthalpy must be due to the local arrangement at the surface. With the formation of an Al $c(2 \times 2)$ sublattice in the first segregation step, all NNN within the top layer are located in the other sublattice (note that the NN are all in the second layer), which exclusively consists of Fe atoms (see figure 6(*b*)). In the next segregation step the second sublattice becomes occupied, whereby eventually all NNN within the top layer are Al atoms and segregation has to work against their repulsion (see figure 6(*c*)). So, both the new Al atom and the substituted Fe atom lose four favoured heterogeneous NNN bonds and gain only

four disfavoured homogeneous NNN bonds. An additional but smaller energetic contribution comes from the repulsive interaction with the increasing concentration of Al atoms in the third layer. In total, the energetic difference between the two segregation steps amounts to at least $16J_{NNN}$, i.e. about 120 meV according to the values given by Sanchez *et al* [41]. A rough estimate from our own data yields a value of the same order of magnitude, 200 meV [22]. Since the segregation enthalpy of the second segregation step is comparably small, this is also a rough estimate of the absolute segregation enthalpy in the dilute limit. Finally, it should be mentioned that for bulk Al concentrations $x > 0.25$ a modified bulk environment must be taken into account and the segregation enthalpy again increases to a value almost as high as the initial one [22]. So, any deviation from a complete Al top layer, as suggested by the LEED analysis for the $Fe_{0.70}Al_{0.30}(100)$ surface, falls beyond the simple interaction model presented above.

5.3. Interpretation of the annealing curves

With the knowledge of the segregation profiles of certain equilibrium phases and the concept of local equilibrium, we can analyse the shape of the annealing curves displayed in figure 3 in more detail. First, it must be considered that the course of these curves is influenced by both the strong Al enrichment in the selvedge and the restoration of the composition in the region below the second layer whereby, however, the latter process is monitored with lower sensitivity due to the attenuation of Auger electrons with depth. Another key to the understanding of the differences between the various annealing curves (besides concentration-dependent diffusion coefficients) is the relative size and location of the Al reservoir, which provides the net amount of material required to restore the stoichiometric equilibrium within the surface. Its importance becomes most obvious for the sample with lowest Al bulk concentration ($x = 0.03$). In this case, the amount of Al accumulation in the top layer corresponding to the $c(2\times2)$ superstructure is equivalent to the Al content of a total of 17 bulk layers, i.e. long-range diffusion processes are required to form the top-layer stoichiometry. As the small bulk concentration allows only small concentration gradients, comparably high annealing temperatures (above 800 K) are necessary to form the enriched selvedge. Within the accuracy of the measurement it is not possible to decide whether there is still some residual depletion in the slab below the top layer as the bulk concentration is only 3%.

Another interesting aspect of the curve for $x = 0.03$ is the initial compositional level right after sputtering, which is about a quarter of that after full annealing, i.e. a quarter of at least half a monolayer of Al. With that assumed to be distributed over the first three layers (roughly equivalent to the AES information depth), an average concentration somewhat higher than $x = 0.03$ results, i.e. the sputtered surface is still enriched in Al. This is in clear contrast to the behaviour of all other Fe–Al samples, where a strong sputter-induced depletion of Al by about a factor of three compared to the bulk is observed. A possible explanation comes from the fact that the reciprocal relation between partial sputter yield and surface concentration holds only for steady-state conditions, i.e. in the limit of infinite sputter times (given that the sputter yield is rather independent of the elemental concentrations). For the moderate sputtering applied, sputter-induced implantation and intermixing effects will play a role, so residues of the original segregation layer can be implanted into deeper layers through ion collisions, so surviving the sputtering process and leading to an increased Al concentration in the altered layer. Of course, a similar competition between sputter-induced Al depletion and implantation must be expected also for the other samples. However, with increasing Al bulk concentration the relative excess caused by segregation diminishes and so Al implantation becomes less and less important. From this argument, the almost identical levels of initial Al concentration for the $Fe_{0.85}Al_{0.15}$ and $Fe_{0.70}Al_{0.30}$ samples might be understandable, too.

Coming back to the transition ranges of the curves, we find that in the case of $Fe_{0.85}Al_{0.15}$ the intermediate $c(2 \times 2)^I$ phase develops best for annealing temperatures around 730 K (see figure 3). From the discussion of the last paragraph, this structure is expected for a concentration around $x = 0.03$ within the underlying altered slab. Since its initial concentration is already above that value, some kind of segregation-induced self-depletion of the slab has to be assumed, which appears reasonable in view of the fact that diffusion is still limited. In the further course of the process of annealing of this sample, the Al concentration of both the actual surface and the subsurface slab increase with temperature in parallel to each other (due to the zero segregation enthalpy in this regime) as outlined above. Therefore, the curve provides a sensitive measure for the progress of the recovery of subsurface stoichiometry. It clearly indicates that annealing temperatures of at least 1100 K are required for the proper equilibration of this sample, much higher than expected. For the $Fe_{0.70}Al_{0.30}$ sample, the Al concentration starts to increase at even lower annealing temperatures, which—besides the higher diffusion coefficients—might be due to the larger reservoir below the (initially rather thin) altered layer. At a temperature of about 700 K, the $c(2 \times 2)^{II}$ phase is best developed, i.e. with highest superstructure spot intensities. Since this superstructure is produced by $D0_3$-like ordering of the subsurface slab, this indicates that ideal $D0_3$ stoichiometry ($x = 0.25$) is reached. Eventually, the stoichiometry $x = 0.30$ is fully restored as reflected by the AES ratio whose related increase is, however, only modest due to electron attenuation as the corresponding process develops only below the outermost (already Al saturated) two layers.

The $Fe_{0.53}Al_{0.47}$ sample still contains a significant amount of Al within the altered layer even right after sputtering. In local equilibrium this would already require an almost complete Al top layer, which is formed (most probably via self-depletion) as soon as short-range diffusion sets in, giving rise to the slow and moderate increase of the Auger ratio between 400 and 600 K. The further development again is exclusively dominated by subsurface stoichiometry restoration which, however, is more drastic than for the other samples and therefore easily visible despite electron attenuation. The scatter in the data in the high-temperature region unfortunately does not allow one to decide at which temperature full equilibration can be assumed. The final re-ascent in the curve above 1100 K can be tentatively assigned to a surface precipitate formation which occurs when a critical concentration is exceeded, as discussed in more detail in the next section. This means that even at these high temperatures, equilibration is not yet complete.

6. From the equilibration process to equilibrium structures—superstructures and precipitates

In the last section we were able to follow the surface equilibration by means of the knowledge of the equilibrium structures of the various samples as retrieved by quantitative LEED analysis. Now we go the reverse way: we try to use the principle of local equilibrium to yield information about the surface structures and segregation profiles developing in the whole concentration regime from the analysis of the equilibration process of a single sample. This procedure is of particular value when surface structures are involved, which due to their complexity are not accessible from quantitative LEED analysis. In the present case of Fe–Al alloys, this applies to the low-index orientations (other than (100)) of B2-ordered FeAl. So, for the (110) surface an incommensurate (IC) superstructure is reported, qualitatively ascribed to a quasi-hexagonal top layer of $FeAl_2$ stoichiometry wherein Al atoms are arranged in a honeycomb-like arrangement around Fe atoms [11, 18, 42]. For the (210) and (111) surfaces, high-order commensurate reconstructions were observed, with periodicities of 3×1 and 3×3 or 6×6 [18] and the (310)-oriented surface was found to even be unstable—i.e. with facets in the [100] direction [18].

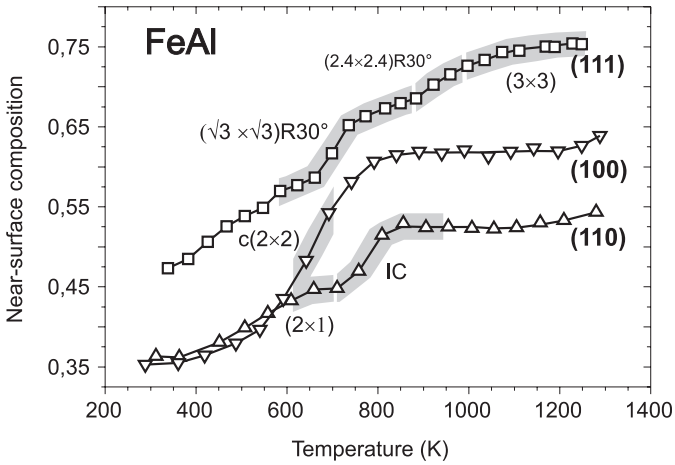

Figure 7. Development of the Auger concentration c_{AES}^{Al} after initial sputtering as a function of annealing temperature for various low-index FeAl surfaces. Ordered superstructures as observed in LEED are given as well, with the corresponding temperature ranges indicated by shading.

In order to interpret the annealing behaviour of these surface orientations, we use the fact that long-range mass transport by bulk diffusion cannot depend much on the surface orientation. So, it can be assumed that the subsurface stoichiometry reached at a certain stage of equilibration (i.e. at a certain annealing temperature) will be more or less the same for all samples. In contrast, near-surface atomic diffusion processes must be expected to depend on the surface orientation, so modifications of the annealing curves can be attributed to them.

6.1. The FeAl(110) surface

Figure 7 displays the equilibration process for the B2-ordered samples $Fe_{0.53}Al_{0.47}(110)$ and $Fe_{0.50}Al_{0.50}(111)$ as monitored by the development of the respective Auger concentration c_{AES}^{Al} with annealing temperature. The quantity c_{AES}^{Al} is calculated from experimental data published earlier [18] using the matrix factor given in section 3. For comparison and to check for the validity of the c_{AES}^{Al}-values derived, data applying to $Fe_{0.53}Al_{0.47}(100)$ are also displayed which, however, were taken for sputtering conditions different to those given in figure 3 (this explains the small modifications in the curve). The high-temperature plateau of the (100) curve corresponding to the B2 phase is at $c_{AES}^{\mathrm{Al}} = 0.62$, whilst the range with the subsurface slab being of $D0_3$ order is $c_{AES}^{\mathrm{Al}} = 0.46$–$0.54$. Consistently, the value calculated for the model of an ideal $Fe_3Al(100)$ surface capped with a full Al top layer results as $c_{AES}^{\mathrm{Al}} = 0.49$. Also consistently, the concentration profile determined by means of LEED for $Fe_{0.70}Al_{0.30}(100)$ leads to $c_{AES}^{\mathrm{Al}} = 0.52$, which is already near the upper edge of the c(2 × 2) region according to the stability range of Fe_3Al in the phase diagram (figure 2(*a*)). So, the evaluation of AES data corroborates the picture drawn from the LEED analyses, i.e. that surface segregation is practically completed already in the $D0_3$ region.

The equilibration curve of the (110) orientation is rather similar to that of the (100) surface with the exception of a small plateau around 700 K, which most likely indicates that top-layer segregation comes earlier to saturation. The curve starts at almost the same Al depletion and reaches a nearly constant concentration level indicative of largely completed equilibration for annealing temperatures also at and above 850 K. From the Auger ratio of this plateau a first-layer Al concentration of $c_{AES}^{\mathrm{Al},1} = 0.60$ results (again under the assumption of ideal

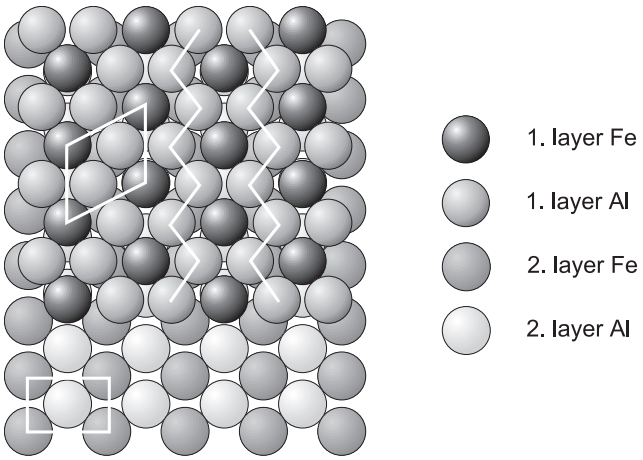

Figure 8. The hard-sphere model (top view) of the IC superstructure of FeAl(110).

bulk-like order below). This is in fair agreement with the value $c_X^{\mathrm{Al},1} = 0.65$ determined by x-ray reflectivity measurements [42] of the IC top layer, and fits equally well to the above-mentioned honeycomb-like $FeAl_2$ model [18, 42], which ideally requires $c^{\mathrm{Al},1} = 2/3 \approx 0.67$ (see figure 8).

In the transition region a 2×1 superstructure is observed in the LEED. It corresponds to the periodicity of a $D0_3(110)$ plane in units of the B2 lattice and so, not surprisingly, it develops exactly in the same temperature interval as the $c(2 \times 2)$ structure of the (100)-oriented sample (figure 7). Indeed, an analysis of LEED intensities for this superstructure clearly proved the existence of a Fe_3Al subsurface slab, though the structure of the first layer could not be resolved [43] which led to the proposal of a locally inhomogeneous top layer [18]. From the almost constant Auger concentration $c_{AES}^{\mathrm{Al}} \approx 0.44$ in the 2×1 regime a top-layer concentration of $c_{AES}^{\mathrm{Al},1} \approx 0.64$ is deduced, when a perfect Fe_3Al slab of $D0_3$ structure is assumed below. This is close to the top-layer composition calculated for the IC structure of the fully annealed surface and so one should expect that the surface has a similar IC top layer already in this state. Consistently, it appears that surface segregation again already comes to a saturation level within the $D0_3$ region and further equilibration proceeds only below, similarly to the findings for the (100) orientation. The fact that in our investigation no IC superstructure spots were visible might be explained by long-range disorder within the top layer caused by some kind of residual defects. This is consistent with investigations reporting 1×1 order [44], probably due to a considerable reduction of IC spot intensities by spurious contaminations. Additional arguments for disorder are given below.

The model of an IC surface structure on a $Fe_3Al(110)$ surface slab or crystal also provides an easy explanation for the structural ambiguity found within the LEED analysis for the top layer. The model is further supported by the literature, where even for a very low Al concentration, i.e. a $Fe_{0.98}Al_{0.02}(110)$ sample, an IC hexagonal superstructure is reported, which undergoes an order–disorder transition around 780 K [45]. This finding points towards a surface structure similar to that predicted above even for very small Al concentrations. Yet, we also have to mention that our model of the surface structure of $Fe_3Al(110)$ is in contradiction to the investigations by Voges *et al* [4]. In their ISS study an almost complete top-layer Al segregation (combined with a temperature-dependent second-layer Al depletion) was determined for a well-annealed $Fe_{0.71}Al_{0.29}(110)$ surface. Such a model would result

in an Auger concentration of at least $c^{\mathrm{Al}}_{AES} = 0.53$, far beyond our limits of error and lying approximately at the level of the completely equilibrated FeAl(110) surface. The aforementioned ISS study also reported some sizable vertical buckling in the top layer which, however, could not be explained consistently [4]. An IC layer, which would inherently exhibit a pronounced vertical rumpling, was not considered.

In order to gain some understanding of the different top-layer structures and segregations of $Fe_3Al(110)$ and FeAl(110) compared to those of the respective (100) surfaces, one has to consider the local bonding geometry in the two surfaces. For (100) surfaces only NNN Fe–Al bonds have to be changed into Al–Al bonds in order to end up with a complete Al top layer. In contrast, replacement of NNN Fe–Al bonds by Al–Al bonds in a (110) layer of Fe_3Al results in a maximum concentration of only 50% Al (corresponding to a FeAl(110) lattice plane). Any further segregating Al atom has to work against four NN Fe–Al bonds within the surface plane and up to two further NN bonds to the second layer, depending on the lattice type below. The high energy costs involved (compared to the gain in surface energy) prevent the realization of a full Al layer. However, Nature finds an alternative solution in rearranging top-layer atoms, favoured by the fact that the second layer is only little corrugated because of being almost close packed, so such a rearrangement will cost comparably little energy. Imagine that there were to be a honeycomb-like layer made up by Al atoms with the vacancy filled by an Fe atom, such that the latter is surrounded by six Al atoms, equivalent to $c^{\mathrm{Al},1} \approx 0.67$. Such a structure would still have three in-plane Al–Al bonds per Al atom. Yet, in order to fit to the observed LEED pattern, this atomic arrangement has to be squeezed in one direction and expanded in the other as displayed in figure 8. Evidently, only two of the three in-plane Al–Al bonds per Al atom remain. The commensurability in one direction also allows one to substantially reduce the number of effective Al–Al bonds between the first and second layer by a proper stacking of the Al–Al zigzag chains above the Fe rows of the second layer; i.e. the reduced symmetry compared to a mere bulk-terminated FeAl surface might provide some excess segregation enthalpy. For a $Fe_3Al(110)$ surface, a bulk-like second layer does not offer complete Al rows any longer but, instead, an alternating linear arrangement of Al and Fe atoms. This certainly allows for local relaxations within the squeezed honeycomb-like structure. However, they cannot be periodic due to the incommensurability in that direction and so give rise to the predicted lateral disorder within the top layer. Finally, for a very dilute random Fe–Al alloy, appearance of Al atoms within the second layer can hardly be expected. In such a case, the main reason for the one-dimensional commensurability of the structure is lacking and, consequently, an ideal hexagonal surface layer may form. One might further speculate whether then even a complete Al top layer might be energetically favourable, so removing discrepancies with other studies [4].

6.2. FeAl(111) and higher-index surfaces

The annealing curve of the FeAl(111) sample displayed in figure 7 differs at a first glance quite remarkably from the others. The Al concentration is much higher even in the as sputtered state and continues to increase up to the highest annealing temperatures, only interrupted by two short plateaus around 600 and 800 K. Though the higher initial Al concentration might be caused by some face-dependent sputter yield or by implantation of Al during moderate sputtering as described above for $Fe_{0.97}Al_{0.03}(100)$, the most probable explanation is that for this sample short-range diffusion is already possible at room temperature, leading to a certain surface segregation. This interpretation is strongly supported by the steep increase of the Auger concentration with temperature right from the beginning, which clearly requires an effective transport mechanism. The two plateaus around 600 and 800 K appear to parallel the

corresponding behaviour of the (110) sample; only the onset of the plateaus is shifted by about 50 K towards lower temperatures. This is easily explainable by higher concentration gradients caused by the higher Al bulk concentration (50% versus 47% in the case of the (110) sample). It is therefore reasonable to assume that the two plateaus again correspond to the development of $D0_3$ and B2 order in the subsurface region. Unfortunately, the LEED patterns for $D0_3$ and B2 order in (111) orientation are both of 1×1 symmetry (only the stacking of Fe and Al layers differs), so there is no direct support for this assumption.

The overall high level of Al concentration, i.e. a strong Al segregation, is mirrored by values of $c^{\mathrm{Al}}_{AES} = 0.57$ and 0.67 calculated for the two plateaus. As in (111) orientation the atoms in the outermost three layers are undercoordinated and so might be involved in the segregation process, one should take this trilayer as an effective top layer. Assuming perfect $D0_3$ and B2 order below it, the same average concentration $c^{\mathrm{Al},tri}_{AES} = 0.75$ results for both plateaus (with, however, the elemental distribution within the trilayer unresolved). The identical average surface stoichiometries for the $D0_3$- and B2-ordered substrates are consistent with LEED investigations, as for both states always the same $(\sqrt{3} \times \sqrt{3})R30^\circ$ surface reconstruction is observed between 570 and 870 K [18] (see figure 7). This superstructure has been found quite recently also for $Fe_3Al(778)$ [46], a surface only 3.5° vicinal to (111). In that STM study, a periodic vacancy structure corresponding to $c^{\mathrm{Al},1} \approx 0.67$ was found for the top layer and, lacking further information, an unreconstructed Fe_3Al bulk was assumed below. In the light of our AES results, however, this top layer can only be part of a more drastic chemical reconstruction induced by segregation. The reader should note that the scenario described is the same as observed for the other low-index surfaces.

Surprisingly, as not observed for the other sample orientations, there is a final increase in Al concentration starting at about 900 K. Since, according to the foregoing discussion, the subsurface region has mostly recovered at that annealing temperature, this increase originates from the actual surface. Reinspection of the phase diagram (figure 2(*a*)) reveals the peculiarity that the B2 phase region does not extend to the ideal composition ($x = 0.50$), at least for low temperatures. Instead, phase separation occurs leading to the formation of $FeAl_2$ precipitates within the FeAl matrix. As such precipitates nucleate preferentially at defects, the presence of a surface is ideal for their development. Their structure may be different from that in the bulk due to epitaxial lattice accommodation; even metastable phases may be epitaxially stabilized. Occasionally, surface precipitates were observed even for bulk concentrations just within the homogeneous phase region [33]. Therefore, we suggest the following model: in the late stage of subsurface equilibration (around 900 K) the altered layer eventually reaches the (surface) phase boundary of the B2 regime. At that point, Al-rich surface precipitates start to grow until they ultimately cover the complete surface, consistent with the observation that a new superstructure with 3×3 (or 6×6) periodicity develops and no residues of the original $(\sqrt{3} \times \sqrt{3})R30^\circ$ superstructure remain. A $(2.4 \times 2.4)R30^\circ$ superstructure observed in a small temperature region at the onset of the final increase in concentration might be interpreted as some kind of precursor for precipitates.

There is additional experimental support for the model described. First, the effect should always occur when the near-surface Al concentration exceeds a certain critical value, more or less independent of the surface orientation. Indeed, a close inspection of the annealing curves for (210)- and (310)-oriented samples [18], which were cut from the very same $Fe_{0.50}Al_{0.50}$ ingot as the (111) specimen, reveals a very similar behaviour, as displayed in figure 9. For all samples, the Al near-surface concentration starts to rise again at about 900 K. Yet, no more information is available for these samples—in particular not as regards details of their ordering behaviour. Another argument comes from the observation that after initial annealing at temperatures above 1000 K, further annealing at lower temperatures (720 K for 1 h) makes

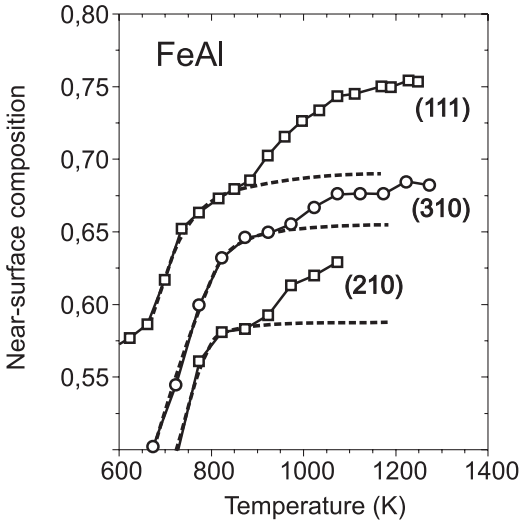

Figure 9. The final stage of the Auger annealing curve for different surface orientations of $Fe_{0.50}Al_{0.50}$. The dashed curves indicate the course of the curves supposed for the absence of precipitate formation.

the Al concentration increase to a value as high as $c_{AES}^{Al} = 0.81$ [18]. As the phase boundary of the B2 regime shifts towards smaller Al concentrations with decreasing temperature, the driving force to form precipitates should be enhanced which, however, needs to be preceded by the chemical restoration of the subsurface slab by high-temperature annealing. Finally, one might speculate that the rise of Al concentration observed for the (100) and (110) surfaces of $Fe_{0.53}Al_{0.47}$ at high annealing temperatures (>1200 K) might also originate from the onset of precipitate formation triggered by the presence of the surface, preventing detailed investigations in this regime of annealing temperatures. Unfortunately, this is also the temperature where Al is already starting to evaporate from the surface. So, without further information available, the extension of the above-described scenario to the (100) and (110) surfaces remains a speculation.

7. Conclusions

Though Fe–Al is an ordering system, its surfaces are dominated by segregation effects. In such a case the equilibrium composition at the selvedge generally depends only little on the exact stoichiometry of the underlying substrate. In particular, essentially the same selvedge structures are found for all low-index surfaces of Fe_3Al and FeAl. As a consequence, the equilibration of sputter-depleted surfaces proceeds in a two-step mechanism. The actual surface is always enriched in Al and thus approaches its equilibrium composition already for rather moderate annealing temperatures through short-range atomic redistribution processes. In contrast, the stoichiometry of the Al-depleted slab below comes to equilibrium only via long-range diffusion from the bulk and thus requires far higher annealing temperatures. During the equilibration process, the structure of the altered subsurface layer is ruled by normal bulk-like atomic interaction and thus strictly follows the phase diagram in the sequence A2 $\rightarrow$ $D0_3$ $\rightarrow$ B2 according to the actual stoichiometry achieved by annealing. In the whole course of structural development, the actual surface is in local equilibrium with the underlying slab. Its structure is determined by qualitatively the same interaction parameters as below and orientation-

dependent features can be explained by the different coordinations of atoms within the lattice planes. In the very late stages of equilibration, the subsurface composition can eventually reach the boundary of the homogeneous phase region and then surface precipitates start to grow. In this special case, their nucleation is a very sensitive indicator for complete equilibration and the surface composition becomes simultaneously a delicate measure for tiny changes of the subsurface stoichiometry. Though our findings were retrieved for a special case, i.e. the Fe–Al alloy, the two-step equilibration model described may apply also to other alloy systems with one of the components having a strong tendency for surface segregation. Moreover, the concept of local equilibrium, which allows one to deduce the equilibrium surface properties of alloys within a whole concentration regime from the investigation of the equilibration process of a single sample, is supposed to be of general validity.

Acknowledgment

This work was supported by the Deutsche Forschungsgemeinschaft (DFG).

References

[1] Polak M and Rubinovich L 2000 *Surf. Sci. Rep.* **38** 127
[2] Derry G N *Handbook of Surfaces and Interfaces of Materials* vol 1, ed H S Nalwa (San Diego, CA: Academic) p 330ff
[3] Blum V, Hammer L, Meier W, Heinz K, Schmid M, Lundgren E and Varga P 2001 *Surf. Sci.* **474** 81
[4] Voges D, Taglauer E, Dosch H and Peisl 1992 *Surf. Sci.* **269–70** 1142
[5] Wang C P, Kim S K, Jona F, Strongin D R, Sheu B-R and Marcus P M 1995 *Surf. Rev. Lett.* **2** 183
[6] Reichert H, Eng P J, Dosch H and Robinson I K 1995 *Phys. Rev. Lett.* **74** 2006
[7] Platzgummer E, Sporn M, Koller R, Forsthuber S, Schmid M, Hofer W and Varga P 1999 *Surf. Sci.* **419** 236
[8] Eltester B, Uebing C, Viefhaus H and Grabke H J 1997 *Fresenius J. Anal. Chem.* **358** 196
[9] Kottcke M, Dötsch B, Hammer L, Heinz K, Müller K and Zehner D M 1997 *Surf. Sci.* **376** 319
[10] Mullins D R and Overbury S H 1988 *Surf. Sci.* **199** 141
[11] Graupner H, Hammer L, Müller K and Zehner D M 1995 *Surf. Sci.* **322** 103
[12] Graupner H, Hammer L, Heinz K and Zehner D M 1997 *Surf. Sci.* **380** 335
[13] Hammer L, Meier W, Heinz K and Niehus H, unpublished
[14] Vitos L, Ruban A V, Skriver H L and Kollár J 1998 *Surf. Sci.* **411** 186
[15] Predel B 1991 *Landolt–Börnstein New Series* Group IV, vol 5a (Berlin: Springer)
[16] Lihl F and Ebel H 1961 *Arch. Eisenhüttenwes.* **32** 483
[17] Rüsenberg M 1986 *Thesis* Düsseldorf University
[18] Hammer L, Graupner H, Blum V, Heinz K, Ownby G W and Zehner D M 1998 *Surf. Sci.* **412–3** 69
[19] Kottcke M, Graupner H, Zehner D M, Hammer L and Heinz K 1996 *Phys. Rev.* B **54** R5275
[20] Blum V, Hammer L, Meier W and Heinz K 2001 *Surf. Sci.* **488** 219
[21] Meier W, Blum V, Hammer L and Heinz K 2001 *J. Phys.: Condens. Matter* **13** 1781
[22] Blum V 2001 *PhD Thesis* Erlangen University
[23] Seah M P and Dench W A 1979 *Surf. Interface Anal.* **1** 2
[24] Tanuma S, Powell C J and Penn D R 1990 *J. Vac. Sci. Technol.* A **8** 2213
[25] Van Hove M A and Tong S Y 1979 *Surface Crystallography by LEED* (Berlin: Springer)
[26] Hall P M and Morabito J M 1979 *Surf. Sci.* **83** 391
[27] Wang C P, Jona F, Gleason N R, Strongin D R and Marcus P M 1993 *Surf. Sci.* **298** 114
[28] Heinz K and Hammer L 1998 *Z. Kristallogr.* **213** 615
[29] Blum V and Heinz K 2001 *Comput. Phys. Commun.* **134** 392
[30] Larikov L N, Geichenko V V and Falchenko V M 1975 *Diffusion Processes in Ordered Alloys* (Kiev: Naukova Dumko) (Reprinted 1981 (New Delhi: Amerind))
[31] Vennegues P, Cadeville M C, Pierron-Bohnes V and Afyouni M 1990 *Acta Metall. Mater.* **38** 2199
[32] Helander T and Agren J 1999 *Acta Mater.* **47** 1141
[33] Viefhaus H 2002 (MPI Düsseldorf), private communication
[34] Atrei A, Bardi U, Torrini M, Zanazzi E, Rovida G, Kasamura H and Kudo M 1993 *J. Phys.: Condens. Matter* **5** L207

[35] Blum R-P, Ahlbehrendt D and Niehus H 1996 *Surf. Sci.* **366** 107
[36] Heinzig M W, Warren O L, Shen Z, Jenks C J, Lograsso T A and Thiel P A 1999 *Mater. Res. Soc. Symp. Proc.* **553** 251
[37] Shen Z, Kramer M J, Jenks C J, Goldman A I, Lograsso T, Delaney D, Heinzig M, Raberg W and Thiel P A 1998 *Phys. Rev.* B **58** 9961
[38] Zurkirch M, Bolliger B, Erbudak M and Kortan A R 1998 *Phys. Rev.* B **58** 14 113
[39] Lawley A and Cahn R W 1961 *J. Phys. Chem. Solids* **20** 204
[40] McLean D 1957 *Grain Boundaries in Metals* (London: Oxford University Press)
[41] Sanchez J M, Pierron-Bohnes V and Mejía-Lira F 1995 *Phys. Rev.* B **51** 3429
[42] Baddorf A P and Chandavarkar S S 1996 *Physica* B **221** 141
[43] Blum V 1996 *Diploma Thesis* Erlangen University
[44] Gleason N R and Strongin D R 1993 *Surf. Sci.* **295** 306
[45] Rüsenberg M and Viefhaus H 1986 *Ber. Bunsenges. Phys. Chem.* **90** 301
[46] Piccolo L and Barbier L 2002 *Surf. Sci.* at press